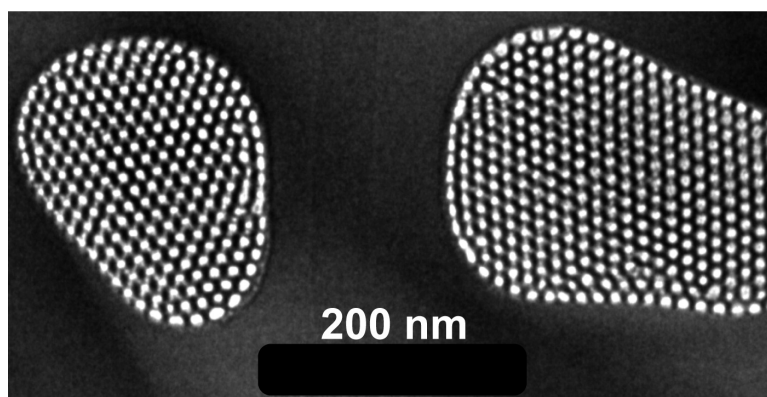


Vertical Columnar Block-Copolymer-Templated Mesoporous Silica via Confined Phase Transformation

Barbara Platschek, Nikolay Petkov, Dieter Himsl, Silvia Zimdars, Zhuo Li, Ralf Köhn, and Thomas Bein

J. Am. Chem. Soc., **2008**, 130 (51), 17362-17371 • DOI: 10.1021/ja803102y • Publication Date (Web): 02 December 2008

Downloaded from <http://pubs.acs.org> on February 8, 2009



More About This Article

Additional resources and features associated with this article are available within the HTML version:

- Supporting Information
- Access to high resolution figures
- Links to articles and content related to this article
- Copyright permission to reproduce figures and/or text from this article

[View the Full Text HTML](#)

Vertical Columnar Block-Copolymer-Templated Mesoporous Silica via Confined Phase Transformation

Barbara Platschek,[†] Nikolay Petkov,[‡] Dieter Himsl,[†] Silvia Zimdars,[†] Zhuo Li,[†] Ralf Köhn,[†] and Thomas Bein^{*†}

Department of Chemistry and Biochemistry and Center for NanoScience (CeNS), University of Munich (LMU), D-81377 Munich, Germany and Department of Chemistry, Materials Section and Supercritical Fluid Centre, University College Cork, Cork, Ireland

Received June 2, 2008; E-mail: bein@lmu.de

Abstract: An efficient method is described for the preparation of phase-pure columnar mesoporous silica nanosystems within the channels of anodic alumina membranes (AAM) via evaporation-induced self-assembly (EISA). Upon the basis of a systematic investigation of the effects of interfacial interactions and different synthesis parameters on the resulting hierarchical mesophase, a salt-induced phase transformation was developed for efficient structural control. Samples with a columnar hexagonal 2D structure along the vertical channels of the AAM can be produced with ionic CTAB as template. However, when nonionic surfactants (Pluronic P123 and Brij 56) are used, samples with a circular hexagonal 2D structure perpendicular to the channels or phase mixtures of circular and columnar orientations are obtained. The behavior of ionic CTAB can be mimicked by adding inorganic salt to the nonionic template precursor solution, thus leading to a phase transformation toward columnar orientation. The distribution between the orientations was determined by means of small-angle X-ray scattering (SAXS) experiments. The effects of other synthesis parameters were also investigated, including temperature, surfactant: silica ratio, and salt composition. Strikingly, calcination-stable mesoporous materials with a columnar orientation exhibiting high mesoporosity and specific surface area were obtained for the first time with such structure directors. The salt-induced phase transformation is an efficient means for achieving a desired hierarchical mesostructure in the confined space of the AAM channels.

1. Introduction

Mesoporous materials with 2D hexagonal order are highly attractive for templated growth of a variety of one-dimensional nanostructures.^{1,2} Nevertheless, potential applications of these structures, for example, in nanoscopic electrical devices, require control over the pore orientation. The evaporation-induced self-assembly (EISA) method³ established to prepare thin periodic mesoporous films on a variety of flat substrates was recently used on porous anodic alumina membranes (AAM), resulting in silica fibers with oriented mesostructures embedded in the AAMs.^{4–7} For future applications of these composite mem-

branes (e.g., as template for the growth of nanowires⁸ or as biomembranes^{9–12}) it is often essential that the AAM channels are completely filled with homogeneously structured phase-pure material.^{13,14} Nevertheless, nonionic surfactants acting as structure-directing agents resulted in 2D hexagonal mesophases with either circular (channels wound around the fiber axis) or mixed circular and columnar (channels parallel to the fiber axis) orientation depending on the synthesis conditions.¹⁵ Preparation of pure columnar mesostructures using nonionic surfactants for the EISA method has not been achieved so far. These difficulties can be understood since, on the one hand, the columnar phase is often kinetically disfavored, implying that the EISA process is slow. Furthermore, with nonionic surfactants the columnar phase does not seem to reflect the thermodynamic minimum

[†] University of Munich.

[‡] University College Cork.

(1) Wight, A. P.; Davis, M. E. *Chem. Rev.* **2002**, *102*, 3589–3614.

(2) Han, Y.-J.; Kim, J. M.; Stucky, G. D. *Chem. Mater.* **2000**, *12*, 2068–2069.

(3) Brinker, C. J.; Lu, Y.; Sellinger, A.; Fan, H. *Adv. Mater.* **1999**, *11*, 579–585.

(4) Yang, Z.; Niu, Z.; Cao, X.; Yang, Z.; Lu, Y.; Hu, Z.; Han, C. C. *Angew. Chem., Int. Ed.* **2003**, *42*, 4201–4203.

(5) Yamaguchi, A.; Uejo, F.; Yoda, T.; Uchida, T.; Tanamura, Y.; Yamashita, T.; Teramae, N. *Nat. Mater.* **2004**, *3*, 337–341.

(6) Wu, Y.; Cheng, G.; Katsov, K.; Sides, S. W.; Wang, J.; Tang, J.; Fredrickson, G. H.; Moskovits, M.; Stucky, G. D. *Nat. Mater.* **2004**, *3*, 816–822.

(7) Lu, Q.; Gao, F.; Komarneni, S.; Mallouk, T. E. *J. Am. Chem. Soc.* **2004**, *126*, 8650–8651.

(8) Petkov, N.; Platschek, B.; Morris, M. A.; Holmes, J. D.; Bein, T. *Chem. Mater.* **2007**, *19*, 1376–1381.

(9) Yamashita, T.; Kodama, S.; Ohto, M.; Nakayama, E.; Hasegawa, S.; Takayanagi, N.; Kemmei, T.; Yamaguchi, A.; Teramae, N.; Saito, Y. *Anal. Sci.* **2006**, *22*, 1495–1500.

(10) Yamaguchi, A.; Yoda, T.; Suzuki, S.; Morita, K.; Teramae, N. *Anal. Sci.* **2006**, *22*, 1501–1507.

(11) Cazacu, A.; Pasc-Banu, A.; Barboiu, M. *Macromol. Symp.* **2006**, *245–246*, 435–438.

(12) Yoo, S.; Ford, D. M.; Shantz, D. F. *Langmuir* **2006**, *22*, 1839–1845.

(13) Ku, A. Y.; Taylor, S. T.; Loureiro, S. M. *J. Am. Chem. Soc.* **2005**, *127*, 6934–6935.

(14) Ku, A. Y.; Taylor, S. T.; Heward, W. J.; Denault, L.; Loureiro, S. M. *Microporous Mesoporous Mater.* **2006**, *88*, 214–219.

(15) Platschek, B.; Petkov, N.; Bein, T. *Angew. Chem., Int. Ed.* **2006**, *45*, 1134–1138.

under these synthesis conditions.^{16,17} Addressing this challenge will permit the use of a variety of surfactants to produce ordered arrays of accessible, straight mesopores with high aspect ratios (maximum length is the thickness of the AAM) and various diameters. Previously, the effect of the geometry of the AAM channels on the formed mesostructure was experimentally studied and modeled by self-consistent field theory.⁶

Structural control in mesophase systems is typically achieved by varying synthesis parameters such as the silica:surfactant ratio,¹⁸ synthesis temperature,¹⁹ or aging time in sol-gel synthesis.²⁰ Though not as extensively investigated, the ionic strength of the synthesis solutions can also play an important role in the process of mesostructure formation. In contrast to nonionic templates, ionic CTAB acting as structure-directing agent leads to exclusive formation of the columnar orientation.¹⁵ A reason for this different behavior might be the relatively strong Coulomb interactions between the ionic template, the charged silica-species, and the alumina wall compared to the weaker hydrogen-bonding interactions between nonionic surfactant, charged silica, and AAM surface. The behavior of the ionic surfactant CTAB was mimicked when cubic mesoporous single crystals were prepared by adding inorganic salt to a nonionic triblock copolymer-containing synthesis solution.²¹ A mechanism for the formation of silicate films at the air/water interface was discussed, proposing that a sphere-to-rod transition in the micellar structure is induced by silicate oligomers gradually replacing water molecules from the surfactant headgroups.^{22,23} This change in micelle conformation was induced by addition of inorganic salt. SBA-15 and aluminum-doped SBA-15 particles with high hydrothermal stability have been produced with a nonionic triblock copolymer by adding sodium chloride to the precursor solution.²⁴ It was assumed that salt-induced dehydration of the polyethylene units creates a local nonpolar environment stabilizing the ordered arrangement of the micelles.

Additionally, increased interaction between silicate species and surfactant headgroups due to the additive electrolyte effect was discussed.^{25,26} An adjustment of the micellar curvature by inorganic salt addition was also reported.^{27–29} Dehydration of the polyethylene oxide headgroups was assumed to reduce the effective headgroup area and therefore lead to decreased micellar curvature. An increase of the micellar radius in mesostructured silica composite films was observed upon increasing the

surfactant: silica ratio and related to changes in the polyethylene oxide headgroup area due to decreased solubilization by water.³⁰ Extraction of water molecules from polyethylene oxide-polypropylene oxide triblock copolymer upon salt addition was demonstrated by a recent ¹H NMR spectroscopy study.³¹ It was demonstrated that micellization is induced when water is removed from the polypropylene oxide moiety, thus decreasing its solubility. Additionally, it was found that water molecules leave the polyethylene oxide shell of the micelles. It was argued that the ions from inorganic salts successfully compete with the polymer chains for the available water of hydration.

Here we examine the influence of inorganic salt addition upon the orientation of the final mesostructure in the confined space of AAMs, aiming at the synthesis of phase-pure columnar hexagonal structure even with nonionic structure-directing agents. Precursor solutions containing P123 {poly(ethylene oxide)₂₀-poly(propylene oxide)₇₀-poly(ethylene oxide)₂₀} or Brij 56 {decaethylene glycol hexadecyl ether} were used. The temperature during the EISA process was also optimized because it can result in different structures when nonionic surfactants are used as templates.³² Finally, the AAM channel surface was hydrophobized by trimethylchlorosilane (TMSCl) treatment prior to synthesis in order to investigate the influence of chemical interactions between the mesostructured materials and the alumina channel wall. The progress of phase transformation was quantitatively followed by 2D small-angle X-ray scattering (SAXS).

2. Experimental Section

The synthesis solutions were prepared by mixing 2.08 g (10 mmol) of tetraethoxysilane (TEOS), 1.8 g (0.1 mol) of water, 3.0 g of hydrochloric acid (0.2 M), and 3.95 g (86 mmol) of ethanol in a polypropylene bottle. The TEOS-containing solution was brought to 60 °C for 1 h for prehydrolysis. In another polypropylene bottle the respective surfactant (750 mg (0.13 mmol) P123 or 906 mg (1.33 mmol) Brij 56) was dissolved in 11.85 g of ethanol. When cooled to room temperature, the respective TEOS- and surfactant-containing solutions were combined and divided in two parts: one-half serving as reference and the other one used after addition of 1 mmol of inorganic salt (58.5 mg of NaCl, 42.5 mg of LiCl, 74.5 mg of KCl, 118 mg of KBr, or 166 mg of KI). The final synthesis solution has a salt:silica ratio of 0.2. For preparation of the additional sample P-21-KIc only 33 mg of KI (0.2 mmol KI) was used, corresponding to a salt:silica ratio of 0.04.

The AAMs (Whatman, 47 mm diameter with about 200 nm channel diameter; these membranes have a plastic ring which prevents spilling of liquid) were placed on a Teflon plate, and 1 mL of the precursor solution was evenly spread on the AAM and left to dry, followed by removal of the silica top layer formed in addition to the intrachannel mesophases (relative humidity while drying = 50–55%). In some cases hydrophobization of the AAMs was carried out by heating the empty AAMs in 8 mL of trimethylchlorosilane (TMSCl) to 70 °C under reflux for 7 h. If the temperature needed to be adjusted, the synthesis was carried out in an oven with controlled relative humidity. The EISA process was carried out at two temperatures: 21 and 30 °C. The chosen difference of 9 °C between the synthesis temperatures is small enough to allow similar drying times. If samples were calcined, the heating rate was 0.5 °C/min, and annealing periods were 10 h at 120 °C, 5 h at 220 °C, and finally 5 h at 400 °C.

- (16) Platschek, B.; Köhn, R.; Döblinger, M.; Bein, T. *ChemPhysChem* **2008**, *9*, 2059–2067.
- (17) Platschek, B.; Köhn, R.; Döblinger, M.; Bein, T. *Langmuir* **2008**, *24*, 5018–5023.
- (18) Zhao, D.; Yang, P.; Melosh, N.; Feng, J.; Chmelka, B. F.; Stucky, G. D. *Adv. Mater.* **1998**, *10*, 1380–1385.
- (19) Cagnol, F.; Grosso, D.; Soler-Illia, G. J. de A. A.; Crepaldi, E. L.; Babonneau, F.; Amenitsch, H.; Sanchez, C. J. *Mater. Chem.* **2003**, *13*, 61–66.
- (20) Grosso, D.; Babonneau, F.; Albouy, P.-A.; Amenitsch, H.; Balkenende, A. R.; Brunet-Bruneau, A.; Rivory, J. *Chem. Mater.* **2002**, *14*, 931–939.
- (21) Yu, C.; Tian, B.; Fan, J.; Stucky, G. D.; Zhao, D. *J. Am. Chem. Soc.* **2002**, *124*, 4556–4557.
- (22) Ruggels, J. L.; Holt, S. A.; Reynolds, P. A.; White, J. W. *Langmuir* **2000**, *16*, 4613–4619.
- (23) Tjandra, W.; Yao, J.; Tam, K. C. *Langmuir* **2006**, *22*, 1493–1499.
- (24) Li, C.; Wang, Y.; Guo, Y.; Liu, X.; Guo, Y.; Zhang, Z.; Wang, Y.; Lu, G. *Chem. Mater.* **2007**, *19*, 173–178.
- (25) Bagshaw, S. A. *Chem. Commun.* **1999**, 1785–1786.
- (26) Yu-Xiang, Y.; Xu-Ping, Q.; Ya-Ru, C.; Xiang-Chen, J. *J. Am. Ceram. Soc.* **2007**, *90* (7), 2050–2056.
- (27) Yu, C.; Fan, J.; Tian, B.; Zhao, D. *Chem. Mater.* **2004**, *16*, 889–898.
- (28) Wang, Y.; Wang, Y.; Yang, C.-M.; Lu, G.; Schüth, F. *Langmuir* **2006**, *22*, 5491–5496.
- (29) Leontidis, E. *Curr. Opin. Colloid Interface Sci.* **2002**, *7*, 81–91.

- (30) Smarsly, B.; Gibaud, A.; Ruland, W.; Sturmayr, D.; Brinker, C. J. *Langmuir* **2005**, *21*, 3858–3866.
- (31) Ma, J.-H.; Guo, C.; Tang, Y.-L.; Wang, J.; Zheng, L.; Liang, X.-F.; Chen, S.; Liu, H.-Z. *Langmuir* **2007**, *23*, 3075–3083.
- (32) Hayward, R. C.; Alberius, P. C. A.; Kramer, E. J.; Chmelka, B. F. *Langmuir* **2004**, *20*, 5998–6004.

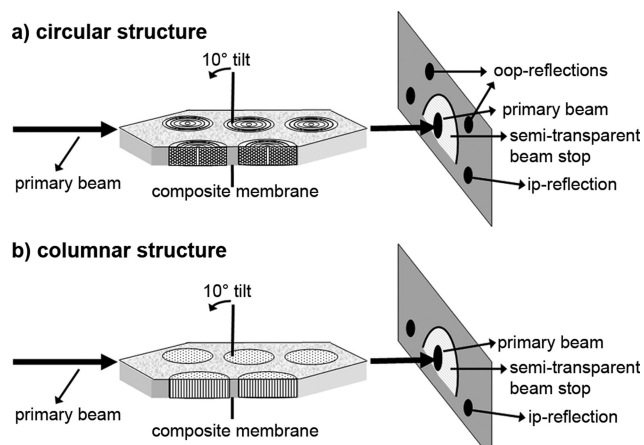


Figure 1. Transmission SAXS setup: The primary beam is weakened by a semitransparent beam stop. Only the upper half of the diffraction pattern is recorded due to the geometry of the instrument. (a) The circular hexagonal phase results in two visible reflections out of the horizontal plane of the primary beam (out-of-plane reflections, oop reflections) and two reflections in the horizontal plane of the primary beam (in-plane reflections, ip reflections). (b) The columnar hexagonal orientation results in only the two ip reflections. A detailed description of the structures and the resulting diffraction patterns is given elsewhere (ref 17).

In the following, the samples are named with capital letters P or B indicating the used surfactants P123 or Brij 56, respectively. The synthesis temperature is denominated by 21 or 30 for 21 and 30 °C. Added salt is given by its sum formula at the end; e.g., P-21-NaCl is a sample synthesized using P123 as structure directing agent at 21 °C with sodium chloride.

The samples were characterized with small-angle X-ray scattering in a transmission experiment with a SAXSess instrument by Anton Paar. Additionally, transmission electron microscopy (TEM) was performed at a JEOL 2011 after dimple grinding and ion milling with a dimple grinder and a precision ion polishing system (PIPS) by Gatan.

The SAXS measurements will result in diffraction patterns with four or two visible first-order reflections (Figure 1) due to the fixed orientation of the mesostructure with respect to the AAM channel walls.^{15–17} The reflections in the horizontal plane of the primary beam (in-plane reflections, ip reflections) correspond to both the circular and the columnar hexagonal orientation. The reflections out of the horizontal plane (out-of-plane reflections, oop reflections) correspond to the circular orientation only. The intensity ratios of the oop to the ip reflections can therefore be used to estimate the distribution between the columnar and the circular phase in the sample. If the oop:ip ratio is zero, only the columnar phase is present in a sample, while a ratio of about 1 is attributed to a pure circular structure.

The oop:ip ratios can only provide a semiquantitative estimate of the phase distribution within one sample due to additional factors such as the measurement geometry (in-plane scattered waves have a longer pathway through the sample than out-of-plane waves which would lead to a systematically lower intensity of the ip reflections). Thus, reference samples were always synthesized, and distinct changes of the oop:ip ratios are always discussed in comparison to the reference.

Determination of the oop:ip ratios was always carried out the same way using an azimuthal angle integration (SAXSquant software by Anton Paar) followed by fitting Gaussians to the resulting one-dimensional peaks and dividing the respective peak intensities. Variations of ± 0.1 of the oop:ip ratio were found to be within the accuracy limit of this method (derived from multiple measurements of one and the same sample). In some samples the ip reflections were partially cut off due to the instrument geometry. Thus, the peak width of the fitted Gaussian is underestimated and

the oop:ip ratio overestimated, sometimes resulting in ratios higher than 1. The oop:ip ratios of these samples are marked with an asterisk (*).

3. Results and Discussion

3.1. Influence of Inorganic Salt Addition. A first set of samples was synthesized at 21 °C. The corresponding diffraction patterns and oop:ip ratios are depicted in Figure 2a–d. A summary of the oop:ip ratios of all prepared samples is given in Table 1.

The reference sample P-21 has an oop:ip ratio of 1.0, while the corresponding sample synthesized with sodium chloride (P-21-NaCl) has an oop:ip ratio of 0.5 (Figure 2a and 2c, respectively). Thus, the reference sample exhibits a much higher fraction of the circular hexagonal phase than P-21-NaCl, which shows more of a columnar orientation. This is confirmed by TEM images of the membrane plane. In the case of a circular orientation the hexagonal order is not imaged in TEM but the circular arrangement of the silica rods is shown (Figure 3a). In the case of the columnar orientation the image is viewed parallel to the silica rods, depicting the hexagonal arrangement of the phase in P-21-NaCl (Figure 3c center). In Figure 3c, showing sample P-21-NaCl, a mixture of both orientations is visible in the TEM image. Some AAM channels are completely filled with either pure circular or pure columnar mesoporous phase. In addition, hybrid structures are observed as well, showing both orientations formed side by side in a single AAM channel (Figure 3c, right side of image). To our knowledge, similar salt-induced phase transformations in confined surfactant-templated mesophase systems have not yet been reported. In agreement with the above discussion, the increased ionic strength of the precursor solutions leads to the formation of less curved mesophases.^{27,28}

Turning now to the samples synthesized using Brij 56 as template, these systems show, both in their respective diffraction patterns as well as in the corresponding TEM images (Figures 2b, 2d, 3b, and 3d), exclusive formation of circular orientation, whether or not inorganic salt was added to the precursor solution. The diffraction spots of B-21-NaCl are weaker than the ones of the reference sample, indicating a reduced order upon salt addition. The reduction of order is confirmed by TEM, the representative image presented in Figure 3d depicting areas of lesser order in comparison to the well-structured circular arrangement of the mesophase in Figure 3b.

3.2. Influence of the Temperature during EISA. Figures 4 and 5 show the data for samples synthesized at 30 °C. The diffraction patterns of the reference samples (synthesized without addition of inorganic salt) using P123 and Brij 56 as templates are depicted in Figure 4a and 4b, respectively. The oop:ip ratio is 1.6* if Brij 56 is used as template, indicating the formation of a pure circular phase. This is also confirmed by the corresponding TEM images shown in Figure 5b. The oop:ip ratio of sample P-30 is 1.3, indicating a circular hexagonal phase. The corresponding TEM images confirm the existence of confined circular phase in sample P-30.

When P123 was used as structure-directing agent and sodium chloride was added to the synthesis solution, the oop:ip ratio derived from the respective diffraction pattern in Figure 4c is 0.3. TEM images confirm the partial transformation toward a columnar orientation; an example is given in Figure 5c. These significant structural changes resemble similar changes with P123 at lower temperature (sample P-21-NaCl depicted in Figures 2c and 3c). Formation of a circular-columnar phase

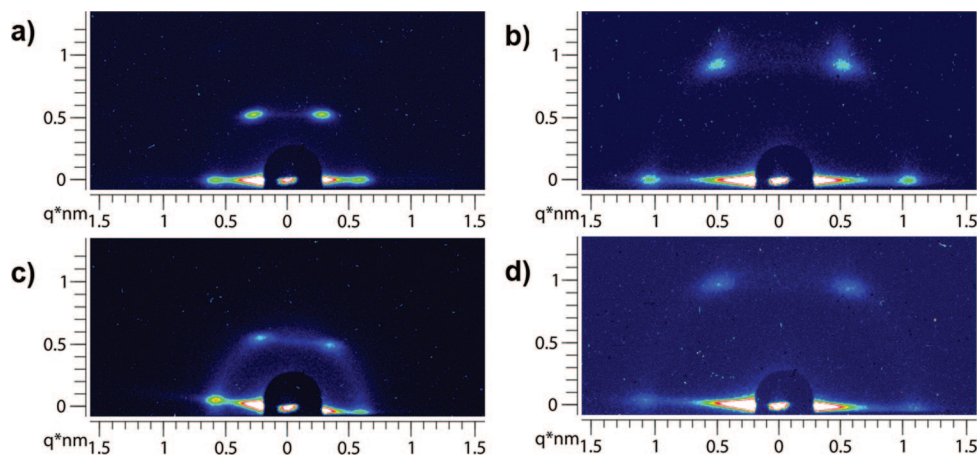


Figure 2. SAXS patterns of samples (a) P-21 (oop:ip = 1.0), (b) B-21 (oop:ip = 1.7*), (c) P-21-NaCl (oop:ip = 0.5), and (d) B-21-NaCl (oop:ip = 1.1) synthesized at 21 °C.

Table 1. Summary of the Data from All Prepared Samples: Sample Name, q Vector, d Spacing Calculated from q , and oop:ip Ratio of Reflections from the Respective Diffraction Patterns^a

sample name	scattering vector q/nm^{-1}	d spacing /nm	lattice constant /nm	oop:ip ratio
P-21	0.62	10.2	11.8	1.0
P-21-NaCl	0.6	10.6	12.2	0.5
P-30	0.62	10.2	11.8	1.3
P-30-calc	0.78	8.1	9.35	1.3
P-30-NaCl	0.6	10.4	12.0	0.3
P-30-LiCl	0.56	11.2	12.9	0.04
P-30-LiCl-calc	0.55	11.5	13.3	0.06
B-21	1.08	5.8	6.7	1.7 ^c
B-21-NaCl	1.08	5.8	6.7	1.1
B-30	1.05	5.9	6.8	1.6 ^c
B-30-calc	1.04	5.9	6.8	2.0 ^c
B-30-NaCl	1.06	5.9	6.8	0.3
B-30-LiCl	1.06	5.9	6.8	0.1 ^c
B-30-LiCl-calc	1.04	6.0	6.9	0.1 ^c
P-21-KCl	0.6	10.4	12.0	0.2
P-21-KBr	0.62	10.2	11.8	0.3
P-21-KI	no structure observed			
P-21-KIc ^b	no structure observed			
P-TMSCl-21	no structure observed			
P-TMSCl-21-NaCl	no structure observed			
B-TMSCl-21	no structure observed			
B-TMSCl-21-NaCl	no structure observed			

^a Calcination is indicated with “calc”. ^b Ic indicates low salt concentration ^c See Experimental Section.

mixture upon salt addition is also observed for sample B-30-NaCl (oop:ip ratio of about 0.3, Figure 4d). The columnar orientation of the mesophase is shown in the corresponding TEM image presented in Figure 5d. Recollect that such influence of the ionic strength was not observed at lower temperature. Brij 56-templated samples show a transformation from circular to columnar orientation only when the synthesis is carried out at elevated temperature (30 °C being the threshold temperature). Hence, the salt-induced phase transformation is a concept valid for both nonionic templates.

3.3. Influence of the Anion. Different inorganic salts were used in the synthesis in order to study their effect on the orientation of the mesostructure in the confined space of the alumina channels. Focusing initially on the influence of the anion, we examined a series of potassium salts with different

counterions in P123-templated mesophases. A diffraction pattern corresponding to a sample synthesized with addition of potassium chloride is shown in Figure 6a. The oop:ip ratio of 0.2 reflects the presence of an almost pure columnar phase in the sample. Thus, the effect of sodium chloride and potassium chloride is comparable.

Figure 6b shows the diffraction pattern from a sample synthesized with potassium bromide instead of chloride. The oop:ip ratio of that sample is similar to the one of P-21-KCl, but the signal-to-noise ratio is decreased compared to the sample synthesized with potassium chloride. When potassium iodide was added to the synthesis solution, no periodic structure was observed in the corresponding diffraction pattern (Figure 6c). When the concentration of potassium iodide was decreased to one-fifth of the original amount, the corresponding diffraction pattern shows a slightly better order (Figure 6d). Hence, bigger anions lead to decreasing order or even distortion of the structure.

3.4. Influence of the Cation. In addition to the effect of the anions, the influence of the alkali cations in the inorganic salts was examined; the corresponding experiments were performed at elevated temperature (30 °C). With lithium chloride, an almost complete transformation toward the columnar orientation could be induced for both surfactants, leaving only negligible amounts of circular phase. The corresponding reference samples P-30 and B-30 with mostly circular orientation have already been discussed in section 3.2. Figure 7a and 7b shows the diffraction patterns of samples P-30-LiCl and B-30-LiCl, respectively. The oop:ip ratios derived from these patterns are 0.04 for P-30-LiCl and 0.1 for B-30-LiCl, indicating a predominantly columnar orientation. The corresponding TEM images shown in Figure 7c for P-30-LiCl and Figure 7d for B-30-LiCl confirm the well-organized columnar hexagonal arrangement of the mesophases. This could be due to small cations leading to a more pronounced transformation toward the columnar phase. Moreover, the specific complexation of hydrated lithium ions with the polyethylene oxide chains of P123 and F127 surfactants is discussed in a recent publication.³³

3.5. Template Removal. The confined mesophase samples were stable upon calcination at 400 °C, while the pore orientation was preserved. For example, the corresponding diffraction patterns of the calcined samples, P-30-calc, P-30-LiCl-calc, B-30-calc, and B-30-LiCl-calc, are shown in Figure

(33) Ganguly, R.; Aswal, V. K. *J. Phys. Chem. B* **2008**, *112*, 7726–7731.

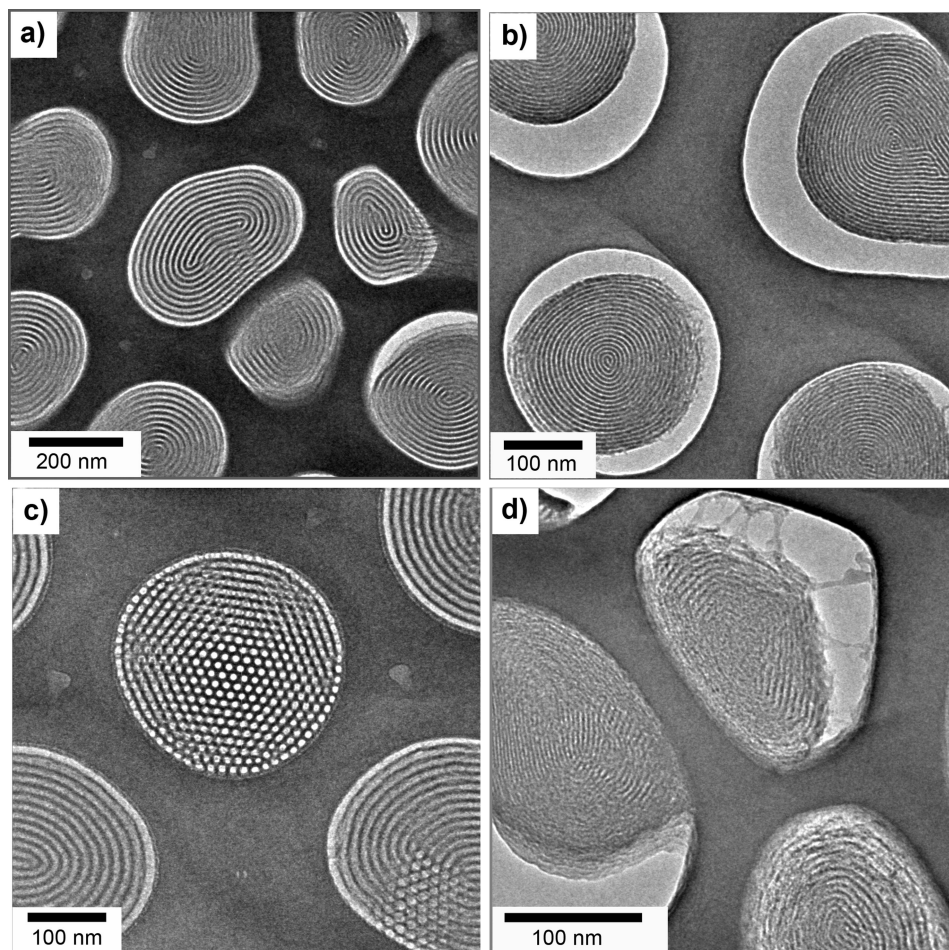


Figure 3. TEM images viewed normal to the AAM surface (plan view). The reference samples (a) P-21 and (b) B-21 exhibit circular orientation. The sample (c) P-21-NaCl shows a mixture of circular and columnar orientation. Sample (d) B-21-NaCl shows a slightly distorted circular hexagonal phase.

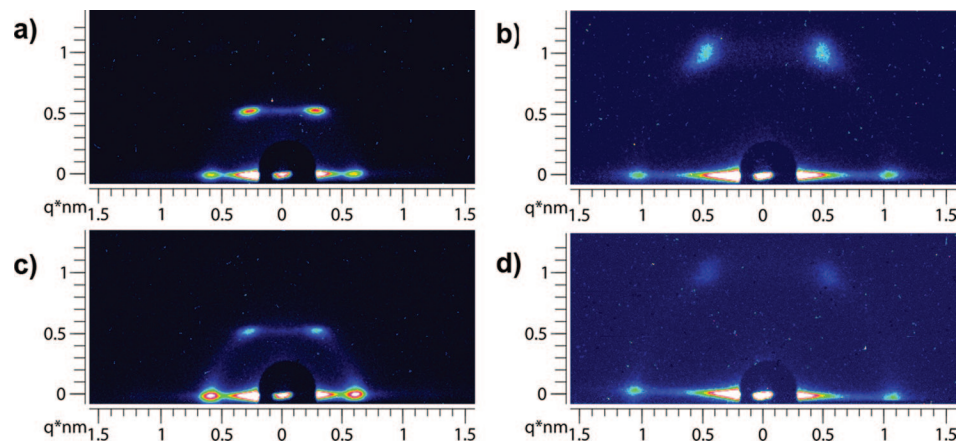


Figure 4. SAXS patterns from samples (a) P-30 (oop:ip = 1.3), (b) B-30 (oop:ip = 1.6*), (c) P-30-NaCl (oop:ip = 0.3), and (d) B-30-NaCl (oop:ip = 0.3) synthesized at 30 °C.

8. Oop:ip ratios are 1.3 and 2.0* for the reference samples P-30-calc and B-30-calc and 0.06 and 0.1 for P-30-LiCl-calc and B-30-LiCl-calc, respectively. It is noticeable that the sample P-30-calc exhibits smaller d spacings after calcination due to shrinkage upon template removal. In contrast, the d spacings calculated from the diffraction patterns for the uncalcined and calcined sample P-30-LiCl(-calc), B-30(-calc), and B-30-LiCl(-calc) are almost identical (see Table 1). This indicates that

addition of inorganic salt not only causes formation of columnar phases but also stabilizes the formed structures against shrinkage.

This observation is confirmed by TEM imaging (Figure 9). Figure 9a shows a corresponding micrograph of sample P-30-calc; an image of sample P-30-LiCl-calc is depicted in Figure 9c. While in sample P-30-calc a set of 9 pores is about 100 nm wide, in sample P-30-LiCl-calc a 100 nm distance corresponds to a set of 6 pores. It is well known that mesoporous films tend

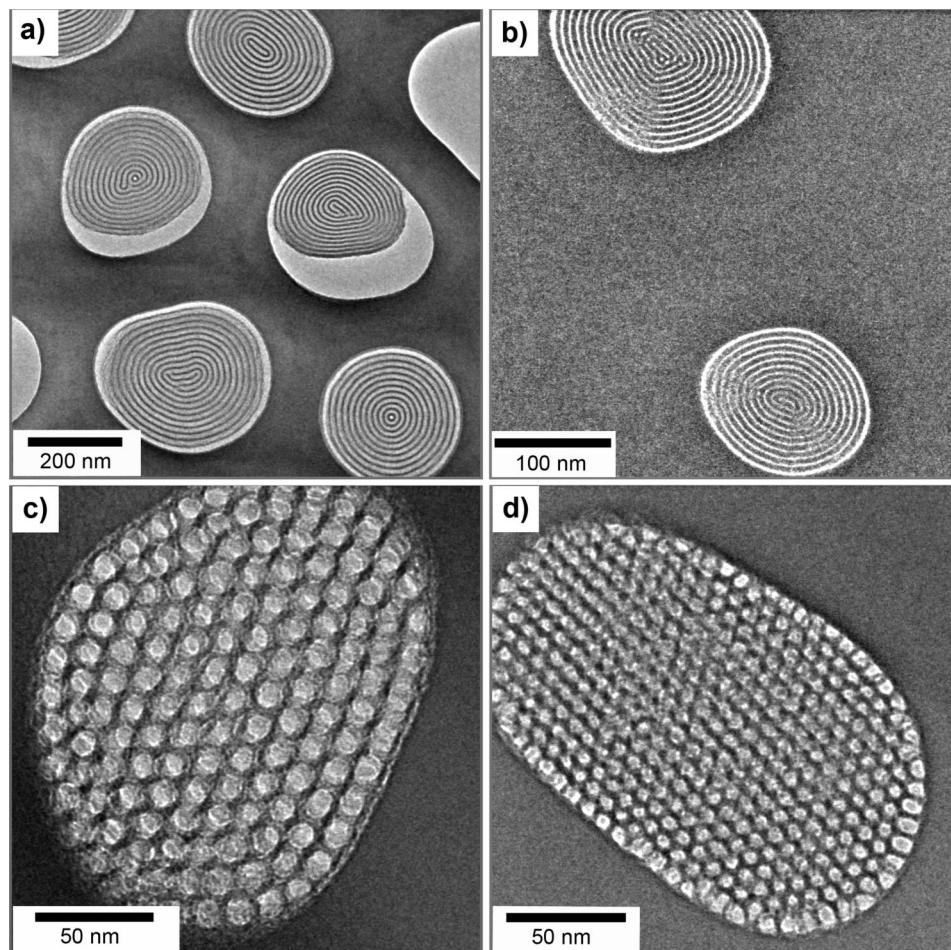


Figure 5. Plan-view TEM images of samples (a) P-30, (b) B-30, (c) P-30-NaCl, and (d) B-30-NaCl. Both reference samples in a and b show exclusively circular orientation of the mesostructure. Images c and d show the columnar hexagonal orientation present in the samples synthesized after addition of inorganic salt.

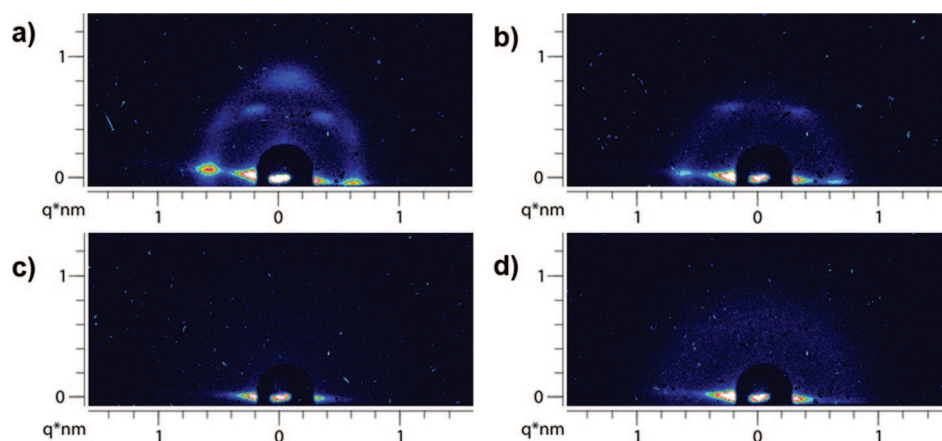


Figure 6. SAXS patterns from samples P-21-KCl, -KBr, -KI, and -KIIc synthesized by adding the same molar ratio (2 mmol per 10 mmol of TEOS) of (a) potassium chloride (oop:ip = 0.2), (b) potassium bromide (oop:ip = 0.3), and (c) potassium iodide to the synthesis solution, and (d) from a sample synthesized with 0.4 mmol of potassium iodide per 10 mmol of TEOS.

to shrink in the direction normal to the substrate surface when they are calcined, resulting in elliptically deformed pores. In the confined environment of the AAM channels the mesoporous material is connected to the alumina channel wall at all sides throughout a length of about $60 \mu\text{m}$, corresponding to the thickness of the AAM. Shrinkage in these systems therefore causes fracture and/or separation from the AAM channel walls.

This effect is even observed in some TEM images of uncalcined samples (the sample preparation and/or electron beam causing the shrinkage). Here, the mesostructured material is detached from one side of the alumina channel wall but still mimicking the shape of the AAM channel (Figures 3b, 3d, and 5a). The location where the mesoporous material detaches from the AAM channel wall is random. Thus, pronounced shrinking of the

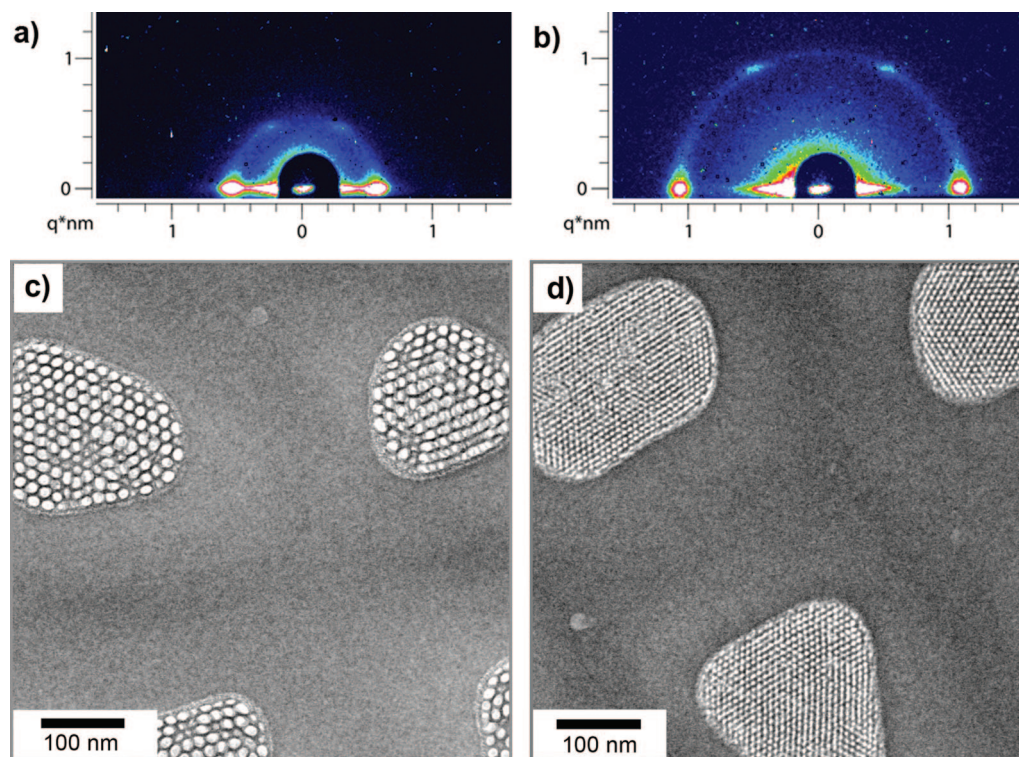


Figure 7. SAXS pattern of samples (a) P-30-LiCl (oop:ip = 0.04) and (b) B-30-LiCl (oop:ip = 0.1) synthesized at 30 °C. Plan-view TEM images of samples (c) P-30-LiCl and (d) B-30-LiCl showing exclusively columnar orientation of the mesostructure.

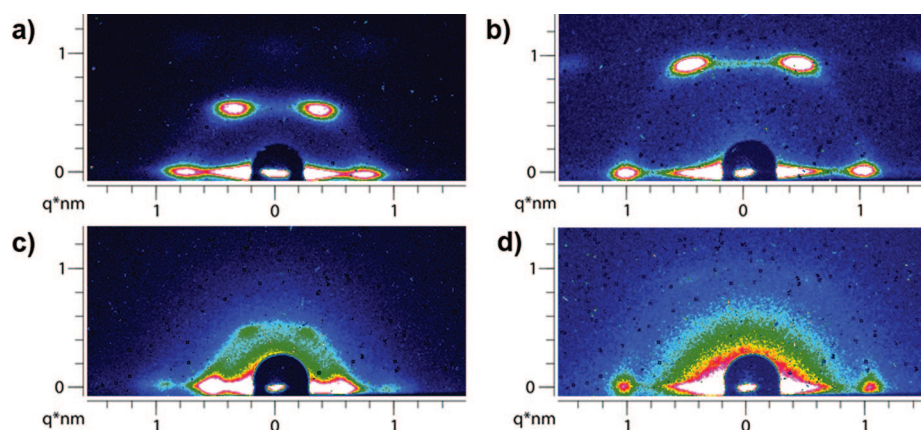


Figure 8. SAXS pattern of samples (a) P-30-calc (oop:ip = 1.3), (b) B-30-calc (oop:ip = 2.0*), (c) P-30-LiCl-calc (oop:ip = 0.06), and (d) B-30-LiCl-calc (oop:ip = 0.1) after calcination at 400 °C. Both structure and orientation are maintained.

structure in sample P-30-calc is not only indicated by the corresponding diffraction pattern (Figure 8a, Table 1) but is directly observed by detachment of the mesoporous fibers from the AAM channel walls in the TEM micrograph of this sample (Figure 9a).

In contrast to the above, it was observed that the columnar phases prepared with the inorganic salts remain attached to the AAM channel surface. Self-assembly within an AAM channel forces the silica template composite to mimic the channel shape. Comparing as-synthesized and calcined samples, the mesopore diameter shows some variations in the as-prepared sample P-30-LiCl (Figure 7c). The material is apparently flexible enough to form slightly smaller or bigger silica template rods to meet the geometric requirements in the confined space. After calcination, the silica phase is much more condensed. The TEM images now show a very regular mesopore structure with consistent

pore diameters, and the mesostructure does not fit the alumina channel as perfectly as before calcination (Figure 9c). The average d spacing represented by the diffraction pattern seems to be unaffected by these small rearrangements. The absence of shrinkage and separation suggests that the inorganic ions increase the chemical interactions between the silica mesophase and the AAM channel surface.

This is supported by another characteristic of the calcined samples synthesized with lithium chloride. It is clearly visible in Figure 9c that there is an amorphous layer of material between the mesostructured silica phase and the surface of the AAM channel. This amorphous layer can reach a thickness of up to about three pore diameters of the mesophase. The same is visible in Figure 9d for the sample synthesized with Brij 56. The TEM images of the uncalcined samples synthesized with salt depicted in Figure 7c and 7d already show a thin amorphous layer at the

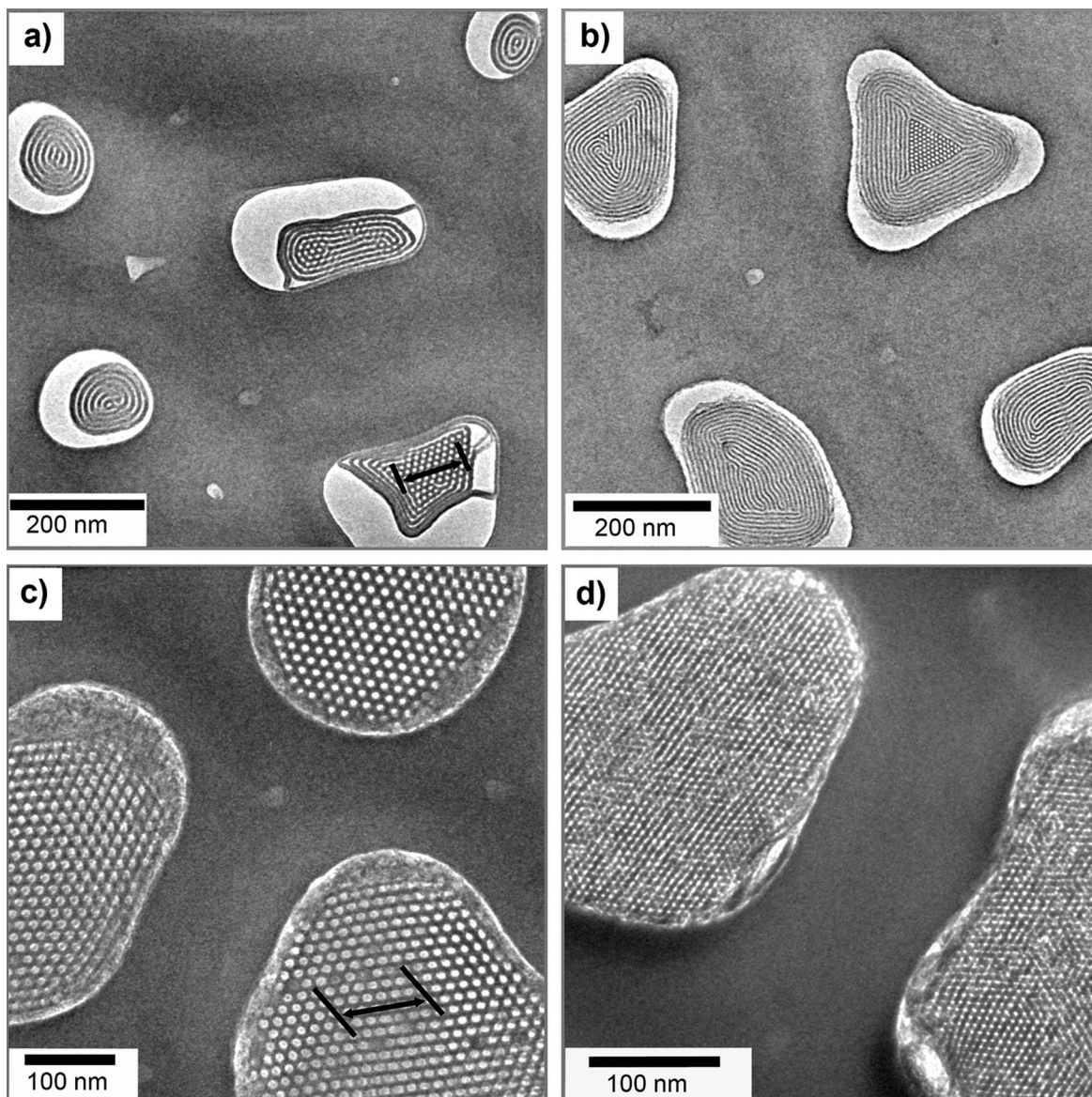


Figure 9. Plan-view TEM images of the calcined samples (a) P-30-calc (inset scale is 100 nm, corresponding to about 9 pores), (b) B-30-calc, (c) P-30-LiCl-calc, and (d) B-30-LiCl-calc (inset scale in (c) is 100 nm, corresponding to about 6 pores). The reference samples show mostly circular orientation and shrinkage of the structure. The samples synthesized with salt exhibit columnar orientation and attachment to the alumina channel wall through an amorphous layer.

mesostructure–AAM interface. This silica layer apparently is expanded during calcination, while the mesophase is getting tighter and more organized, possibly filling the gap between mesostructure and AAM channel surface. Such a layer of amorphous silica is not visible in calcined samples with circular structures prepared without addition of inorganic salt. Instead, in those samples the silica mesophase tends to detach from the alumina wall, leading to large gaps between the wall and the mesostructure. This is an important aspect regarding potential applications of these composite membranes, e.g., as templates for the growth of nanowires. For such applications it is often essential that the AAM channels are completely filled with material.

The interactions between the silica species and the alumina channel wall seem to be not only important for the formation of a certain orientation but also crucial for the formation of a mesostructure as such. When the surface of the AAM channels was made hydrophobic by modification with TMSCI, only unstructured material was found to form during EISA.

3.6. Mesoporosity. Nitrogen adsorption/desorption isotherms and respective pore-size distribution curves of the samples B-30-calc, B-30-LiCl-calc, P-30-calc, and P-30-LiCl-calc are shown in Figure 10. Samples B-30-calc and P-30-calc exhibit pure circular orientation of the hexagonal phase (oop:ip ratios of 2.0* and 1.3, respectively). The samples synthesized with LiCl (B-30-LiCl-calc, P-30-LiCl-calc) represent rather pure columnar hexagonal structures. All samples show type IV isotherms including the monolayer–multilayer adsorption and capillary condensation. Hysteresis loops are observed in the adsorption and desorption cycle around the capillary condensation, typical for mesoporous materials with cylindrical mesopores.

Specific surface areas calculated by the BET method and pore diameters corresponding to the maxima in the respective pore size distribution curves are given in Table 2 for each sample. The pore size distributions are calculated based on the adsorption branch and the DFT method. Note that the specific surface areas in Table 2 are measured with the ground alumina/silica

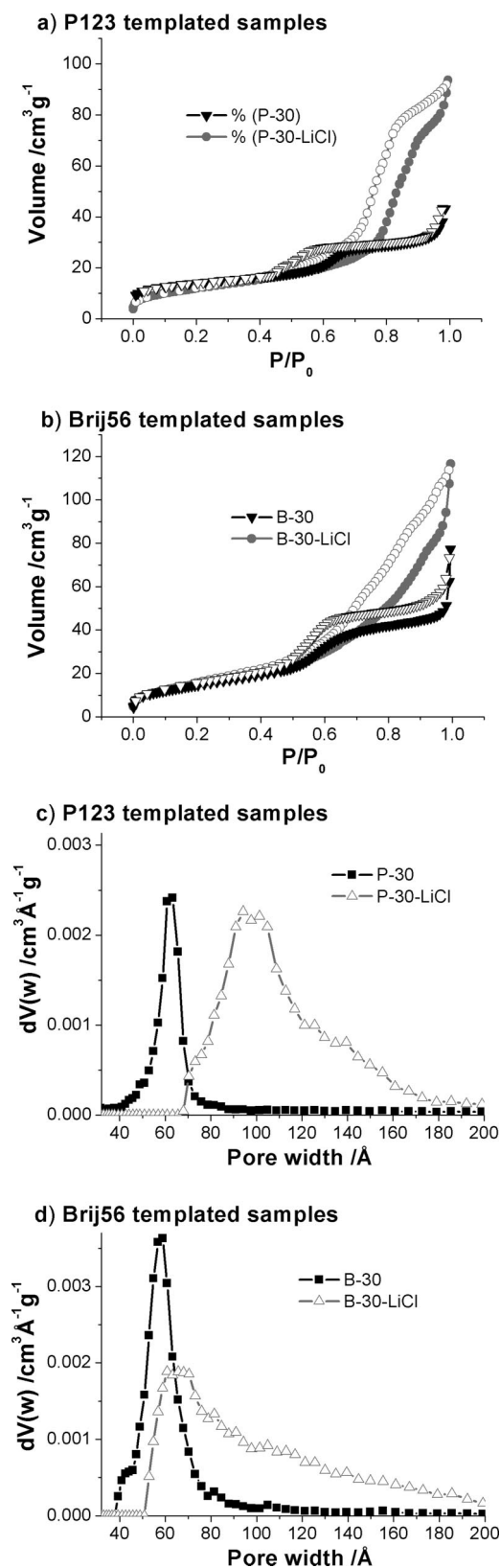


Figure 10. Nitrogen adsorption/desorption isotherms and the respective pore size distributions based on the adsorption branch and the DFT method of samples P-30-calc (circular), and P-30-LiCl-calc (columnar) (a,c) as well as B-30-calc (circular) and B-30-LiCl-calc (columnar) (b,d). Open symbols represent the desorption branch and filled symbols the adsorption branch. Pore size distributions based on the desorption branch are given in the Supporting Information (Figure S1).

Table 2. Sorption Characteristics of Circular and Columnar Samples Prepared with Brij 56 and P123

sample name	oop:ip ratio	specific surface area/m ² g ⁻¹ ^a	pore diameter/nm
P-30-calc	1.3	48	6.3
P-30-LiCl-calc	0.06	43	9.8 (and shoulder)
B-30-calc	2.0*	54	5.9
B-30-LiCl-calc	0.1	55	6.6 (and tailing)

^a Specific surface area of the alumina/silica composite (ground powder).

composite powder. Thus, the surface area (m²/g) is not to be compared with surface areas measured from pure mesoporous material.³⁴

While distribution curves for the circular samples B-30-calc and P-30-calc exhibit narrow peaks at smaller pore diameters, the peaks are broadened and shifted to higher values for the samples with columnar phases. In sample B-30-calc, which is a Brij 56-templated sample with circular orientation, one comparatively sharp peak with a maximum at 5.9 nm pore diameter is visible, while the sample B-30-LiCl-calc with pure columnar orientation exhibits a broader peak with a maximum at 6.6 nm pore diameter and an additional tail ranging from about 8 to 18 nm.

A similar effect is observed in samples synthesized with P123. The circular structure (P-30-calc) shows a pore-size distribution with one narrow peak having a maximum at 6.3 nm. The pure columnar structure found in P-30-LiCl-calc shows only one broad peak with a maximum at 9.8 nm pore size plus a shoulder ranging from 13 to 18 nm. Thus, sorption data confirm that addition of inorganic salt not only promotes formation of columnar phases but also leads to enhanced stability of the structures against shrinkage during calcination.

A broader pore-size distribution with a tail toward larger diameters is observed for the pure columnar phases obtained upon addition of salt. The tails between 8 and 18 nm in sample B-30-LiCl-calc and 13 and 18 nm in sample P-30-LiCl-calc are attributed to the occasional merging of pores. TEM images of different locations of the calcined samples reveal that there are some areas where the silica walls between the mesopores are ruptured and pores are merged (Supporting Information, Figure S2). Larger pore diameters and the merging of pores support the earlier statement that the interactions of the mesophase with the alumina channel wall are increased due to addition of inorganic salt. In the circular phase, mechanical stress during template removal leads to detachment from the channel walls,

(34) The porosity of the alumina membrane is 25–50% according to the manufacturer. For the silica material around 50% of the volume are pores, estimated from TEM micrographs. The density of the alumina (without pores) is about 3.98 g/cm³ (α-alumina), and the density of the silica (without pores) is about 2.65 g/cm³ (quartz). Hence, from 1 cm³ composite material, 0.75–0.5 cm³ originate from alumina material while only 0.125–0.25 cm³ is silica material. With the respective densities, 1 cm³ composite contains 0.33–0.66 g silica and 2.98–1.99 g alumina depending on the original membrane porosity (25–50%). This corresponds to a silica content of 10–25 wt % in the composite. Thus, only one-fourth to one-tenth of the specific surface area of pure mesoporous material can be obtained for the composite (highly ordered SBA-15 materials show specific surface areas of 500–800 m²/g; for the corresponding composite, surface areas between 50 and 200 m²/g can be expected). Note that the discussed weight correction does not take into account possible incomplete filling of the AAM, pore-blocking effects due to the long channel system, or reduction of the surface area due to formation of relatively large pores in the confined environment (see text).

while the columnar phase remains attached to the alumina, showing larger pore diameters and in some cases rupture of the silica walls.

4. Conclusions

In this work we have demonstrated that AAM-confined mesostructures with columnar instead of circular orientation can be formed with nonionic surfactants as structure-directing agents upon increasing the ionic strength of the respective precursor solutions. Formation of an amorphous silica layer at the interface to the alumina channel walls indicates increasing chemical interactions with these walls upon addition of inorganic salt. Accordingly, no mesophase was formed with any of the different precursor solutions inside the channels of an AAM that was hydrophobized by surface modification. We show that small cations lead to a more pronounced formation of the columnar phase and that large anions can lead to phase distortion. The temperature during the EISA process plays a key role in the

salt-induced phase transformation. The confined mesostructures were found to be stable upon calcination at 400 °C, resulting in mesoporosity with relatively high specific surface areas and pore size distributions reflecting the different pore structures. The extensive structural control achieved for these hierarchical periodic mesoporous systems will provide the foundation for diverse applications in inclusion chemistry and molecular separations.

Acknowledgment. The authors thank the Deutsche Forschungsgemeinschaft (DFG) for financial support through the SFB 486 and the NIM cluster.

Supporting Information Available: Figures showing pore size distributions of several samples and TEM images of LiCl-containing mesoporous silica in AAM membranes. This material is available free of charge via the Internet at <http://pubs.acs.org>.

JA803102Y